Contract No:

This document was prepared in conjunction with work accomplished under Contract No. DE-AC09-08SR22470 with the U.S. Department of Energy.

Disclaimer:

SRNL
SAVANNAH RIVER NATIONAL LABORATORY
OPERATED BY SAVANNAH RIVER NUCLEAR SOLUTIONS

October 2, 2014 SRNL-STI-2014-00467

Subject: SRNL CRP Progress Report

From: J. W. Amoroso
J. C. Marra

Development of Melt Processed Ceramics for Nuclear Waste Immobilization

1.0 Abstract

A multi-phase ceramic waste form is being developed at the Savannah River National Laboratory (SRNL) for treatment of secondary waste streams generated by reprocessing commercial spent nuclear. The envisioned waste stream contains a mixture of transition, alkali, alkaline earth, and lanthanide metals. Ceramic waste forms are tailored (engineered) to incorporate waste components as part of their crystal structure based on knowledge from naturally found minerals containing radioactive and non-radioactive species similar to the radionuclides of concern in wastes from fuel reprocessing. The ability to tailor ceramics to mimic naturally occurring crystals substantiates the long term stability of such crystals (ceramics) over geologic timescales of interest for nuclear waste immobilization [1]. A durable multi-phase ceramic waste form tailored to incorporate all the waste components has the potential to broaden the available disposal options and thus minimize the storage and disposal costs associated with aqueous reprocessing.

2.0 Introduction

The traditional method for HLW immobilization is to form borosilicate glass by a vitrification process, a practice currently used for defense and commercial waste [1]. In contrast, our objective is to use a traditional melting process to crystallize ceramics from the melt. Compositions are designed based on combinations of the waste and additives to target desired hollandite, perovskite, and pyrochlore phases upon melting. Elements with a +3 or +2 valance form perovskite ($(A^{+2})TiO_3$) and pyrochlore ($(A^{+3})_2Ti_2O_7$) type phases [2, 3]. Zirconium (+4 valence) partitions to a zirconolite ($CaZrTi_2O_7$) phase [4]. Cs and Rb elements partition to a hollandite structure based on the general formula $Ba_xCs_yM_zTi^{+4}{}_{8-z}O_{16}$ where z = 2x+y for trivalent cations and z = x+y/2 for divalent cations for charge compensation [5-7].

Multiphase ceramics targeting an assemblage of titanate-based phases have been successfully demonstrated to incorporate various radioactive waste elements into a number of crystalline phases. Most notable are the synthetic rock (SYNROC) family of minerals developed in the 1980s that have been primarily produced by hot-pressing [2,3]. Melt processing of waste forms is considered advantageous over the conventional solid-state synthesis methods given that melters are currently in use for HLW vitrification in several countries, greatly facilitating the technology readiness of ceramic waste forms, and

melter technology can reduce the potential for airborne contamination during pretreatment as compared to processes involving extensive powder handling operations.

There have been several comparative studies of crystalline ceramic waste forms produced by hot pressing and inductive melting [4,5]. These prior studies have indicated that the specimens fabricated by melting and solid state sintering exhibited similar mineral compositions. Under oxidizing processing conditions, attempts to make single phase hollandite (the host phase for Cs) ceramics are difficult and secondary metastable Cs containing phases are formed [6]. In particular, water-soluble cesium molybdate phases observed in melt processing Mo containing waste in air are undesirable. It has been demonstrated that these secondary phases can be suppressed by controlling the starting composition and the Ti^{3+}/Ti^{4+} during processing. Metal powder (Ti) additions to the batch material or hot pressing in graphite have been shown to be effective methods for controlling the redox conditions during sintering [7,8].

The present work is aimed at improving composition and processing parameters to alleviate detrimental features in the final product such as low-durability phases and to improve the melt-processing behavior. In addition, there is particular interest regarding the characteristics of phase formation and elemental partitioning in melt processed ceramic composites. Ultimately, the intent is to demonstrate the feasibility of melt processing technology to produce multiphase waste forms with desirable phase composition. This report summarizes recent developments of melt processing ceramic waste forms.

3.0 Composition Development

3.1 Projected Waste Composition

The waste composition that formed the basis for the development and testing is given in Table 3-1. Noble metals, minor actinides and Tc were removed for cost and handling reasons. The MoO_3 targeted in this work was based on one possible reprocessing flowsheet, but other variants exist and more will be developed based in part on waste form studies such as this. Because this work incorporated varying redox conditions and previous results indicated large concentrations of MoO_3 inhibited desired phase formation under oxidizing conditions, the MoO_3 concentration was targeted at 3 wt. % to simplify comparison among samples.

Table 3-1. Projected and re-normalized waste composition targeted in this study

Group	Fuel[a]	SRNL[b]	Fuel[c]
Alkali	7.6	13.4	9.6
Alkaline Earth	8.3	12.9	10.6
Lanthanides	33.1	51.8	42.0
Actinides	4.0	-	-
Noble Metals	14.6	-	-
MoO_3	13.7	3.4	17.4
ZrO_2	13.7	12.1	17.4
TcO_2	2.7	-	-
Others	2.4	6.3	3.0
Total	100	100	100

[a]Projection

[b]Does not include corrosion and process products

[c]Renormalized to exclude corrosion and process products

3.2 Hollandite Phase Development

Cs is one of the more problematic fission product radionuclides to immobilize due to its high volatility, ability to form water soluble compounds, and its mobility in many host materials. There are natural analogues of hollandite including ankagite, found in dolomitic marble in the Apuan Alps in Tuscany, Italy which demonstrate the long term stability of these crystal structures over geologic timescales [9]. The hollandite group of minerals has the formula $A_xB_yC_{8-y}O_{16}$ where the B and C cations are surrounded by octahedral configuration of oxygen [10]. In the hollandite structure, columns of four pairs of edge sharing octahedra connected to each other on the corners form tunnels running parallel to the short crystal axis. The tunnel cross-section is generally square, but will distort as a rhombus depending on the particular Hollandite symmetry which can be either monoclinic (rhombus) or tetragonal (square) depending on the radius ratio of the A to B site cations. Figure 1 depicts a two-dimensional schematic of the tetragonal hollandite structure. In hollandite structures used for nuclear waste incorporation, the A site is occupied by Cs/Rb and Ba, the B site by Al^{3+} and Ti^{+3}, and the C site by Ti^{+4} resulting in the general formula of $(Ba_xCs_y)(Ti,Al)^{+3}_{2x+y}(Ti^{+4}_{8-2x-y})O_{16}$ [11].

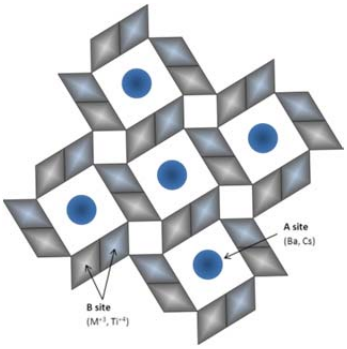

Figure 3-1. Idealized two-dimensional [001] projection of the tetragonal hollandite structure showing octahedra pairs lining the tunnels and A site cation positions.

4.0 Single Phase Hollandite Crucible Studies

Cs-containing hollandite ceramics with Cr additions of the form $Ba_{1.0}Cs_{0.3}A_{2.3}Ti_{5.7}O_{16}$ (A = Cr, Fe, Al) were developed precursory to multiphase work. Cr-containing hollandite was developed to exploit the relative thermodynamic stability of Cr oxides and the Cr ionic radius that is less than Fe^{3+} but greater than Al^{3+}. Three nominal hollandite compositions, $Ba_{1.0}Cs_{0.3}Cr_{2.3}Ti_{5.7}O_{16}$ – referred to as Cr-Hol, $Ba_{1.0}Cs_{0.3}Cr_{1.0}Al_{0.3}Fe_{1.0}Ti_{5.7}O_{16}$ – referred to as CAF-Hol, and $Ba_{1.0}Cs_{0.3}Fe_{2.3}Ti_{5.7}O_{16}$ – referred to as Fe-Hol were prepared and characterized. In addition, the waste stream is anticipated to contain MoO_3 which is known to preferentially react with Cs_2O and it is recognized that reducing atmospheres are a proven method to suppress Cs-Mo secondary phase formation. Based on that expectation, a variety of reducing conditions were evaluated including the use of solid state reducing agents (Ti/TiO_2) and reducing gas environments ($1\%H_2/Ar$). The approach in this precursory work was to study an additive (Cr) that promoted single phase hollandite formation and Cs incorporation across a wide range of redox conditions thus resulting in a flexible Cs immobilization host material that could be incorporated into a multiphase ceramic.

4.1 Preparation and Processing

For each composition, stoichiometric amounts of reagent-grade oxide and carbonate powders (99.5 % purity) to make 100 g of hollandite material were combined in a 500 ml plastic bottle with zirconia milling media, filled 2/3 full with deionized water, and agitated in a tumbler mixer for 1 hour. Subsequently, each slurry was poured into a separate pan along with additional rinse water used to collect any batch material remaining on the milling media and bottles. Each pan was transferred to an oven where the slurry was dried for several days at 90°C. The dried material was bagged and used as feed stock for synthesis experiments.

Approximately 20 g samples feed stock was placed loosely into a covered alumina crucible. The samples were heated in air and in 1% H_2 (99% Ar) reducing atmosphere. Ti metal and TiO_2 additions were made to some batches prior to synthesis. For those samples, prepared mixtures of 2.0 wt. % Ti metal and 7.0 wt. % TiO_2 were manually mixed into each batch. Samples were heated at approximately 15 K/min, held at 1500 °C for 20 minutes, and furnace cooled (powered off furnace). Table 4-1 summarizes the experimental matrix including hollandite composition, solid state sintering additives and processing conditions used in this work.

Table 4-1. Composition, Additive, and Processing Atmosphere Experimental Matrix

Target Hollandite Composition	Additive	Atmosphere	Short Identifier
$Ba_{1.0}Cs_{0.3}Fe_{2.3}Ti_{5.7}O_{16}$	Ti-TiO_2	Air	Fe-SPH-Ti
		Reduced (1%H_2)	Fe-SPHR-Ti
	n/a	Air	Fe-SPH
		Reduced (1%H_2)	Fe-SPHR
$Ba_{1.0}Cs_{0.3}Cr_{2.3}Ti_{5.7}O_{16}$	Ti-TiO_2	Air	Cr-SPH-Ti
		Reduced (1%H_2)	Cr-SPHR-Ti
	n/a	Air	Cr-SPH
		Reduced (1%H_2)	Cr-SPHR
$Ba_{1.0}Cs_{0.3}Cr_{1.0}Al_{0.3}Fe_{1.0}Ti_{5.7}O_{16}$	Ti-TiO_2	Air	CAF-SPH-Ti
		Reduced (1%H_2)	CAF-SPHR-Ti
	n/a	Air	CAF-SPH
		Reduced (1%H_2)	CAF-SPHR

4.2 Results

4.2.1 X-ray diffraction

The phases identified by XRD are summarized and presented in Figure 4-1. All Cr-Hol samples were single phase except the sample heated in air to which Ti/TiO_2 was added, which contained excess rutile (TiO_2). This was not unexpected, as excess TiO_2 was intentionally added and similar results have been reported by other groups. All CAF-Hol samples exhibited a major hollandite phase, but also contained minor titanate phases. In contrast, the Fe-Hol samples, although exhibiting a major hollandite phase, also contained several parasitic phases including titanatates and aluminates. The majority of the detected parasitic phases would be expected to be durable. However, one phase, $CsAlTiO_4$ was also detected and is known to adversely affect Cs retention when subjected to a durability test.

Table 4-2. Summary of Crystalline phases determined from X-ray Diffraction XRD measurements and Energy Dispersive X-ray Spectroscopy EDAX elemental analysis

Short ID	Major Phase[1]	Minor Phase(s)[2]	Processing Conditions
Fe-SPH	Hollandite	$Fe_2Ti_3O_9$; $CsTiAlO_4$	Air
Fe-SPH-Ti	Hollandite	$Fe_3Ti_3O_{10}$; $CsTiAlO_4$	Air w/Ti-TiO_2
Fe-SPHR	Hollandite	$BaFe_{12}O_{19}$; $CsTiAlO_4$; $FeAl_2O_4$	1% H_2
Fe-SPHR-Ti	Hollandite	Al_2O_3; $FeAl_2O_4$	1% H_2 w/Ti-TiO_2
Cr-SPH	Hollandite		Air
Cr-SPH-Ti	Hollandite	TiO_2	Air w/Ti-TiO_2
Cr-SPHR	Hollandite		1% H_2
Cr-SPHR-Ti	Hollandite		1% H_2 w/Ti-TiO_2
CAF-SPH	Hollandite		Air
CAF-SPH-Ti	Hollandite	TiO_2	Air w/Ti-TiO_2
CAF-SPHR	Hollandite	Fe_2TiO_4; $BaFe_{12}O_{19}$; $CsTiAlO_4$	1% H_2
CAF-SPHR-Ti	Hollandite	Fe_2TiO_4	1% H_2 w/Ti-TiO_2

[1] Many hollandite phases exist in the literature. In general, the following PDF files were used to identify the hollandite phases: Fe: 00-051-1900; Cr: 00-039-0352, CAF: 01-076-3178.

[2] The following PDF files were used to identify the minor phases: TiO_2: 00-021-1276; $BaFe_{12}O_{19}$: 00-039-1433; Fe_2TiO_4: 00-034-0177; $FeAl_2O_4$: 01-086-2320; $CsTiAlO_4$: 04-009-3837 $Fe_3Ti_3O_{10}$: 00-047-0421; $Fe_2Ti_3O_9$: 00-0407-1777; Al_2O_3: 00-005-0712

4.3 Electron microscopy

Microstructure and phase purity of the single phase hollandite compositions are shown in Figure 4-1. Overall, the observed microstructures confirm the XRD results indicating that the Cr-hol samples were single hollandite phase, the CAF-Hol samples exhibited a major hollandite phase accompanied by minor phases, and the Fe-hol samples were multiphase. Semi-quantitative EDS confirmed the composition of many of the various phases as shown in Figure 4-1. CAF-Hol samples were characterized further with high resolution transmission electron microscopy (HRTEM) and SEM. Figure 4-2, which shows the HRTEM results for the CAF-Hol sample heated in air, indicated the hollandite phase was highly crystalline and contained all the expected elements including Cs. The selected area diffraction (SAD) pattern shown in the inset was indexed to a tetragonal hollandite phase. Elemental maps of the Al, Cs, Fe, and Cr concentrations of Cr/Al/Fe-hol samples heated in 1%H_2 *with and without* Ti/TiO_2 are presented in Figure 4-3. The Cr-rich phase was identified as the primary hollandite phase. Fe partitioned mainly to a reduced titanate phase in both samples, but was also distributed along hollandite grain boundaries in the sample processed *without* Ti/TiO_2 additions. The Cs was associated with the Al in the CAF-Hol sample heated in 1%H_2 *without* Ti-TiO_2 and is the characteristic bright phase in SEM identified as $CsAlTiO_4$. In contrast, the Cs appeared more distributed in the CAF-Hol sample heated under the same atmosphere, but *with* Ti/TiO_2 additions.

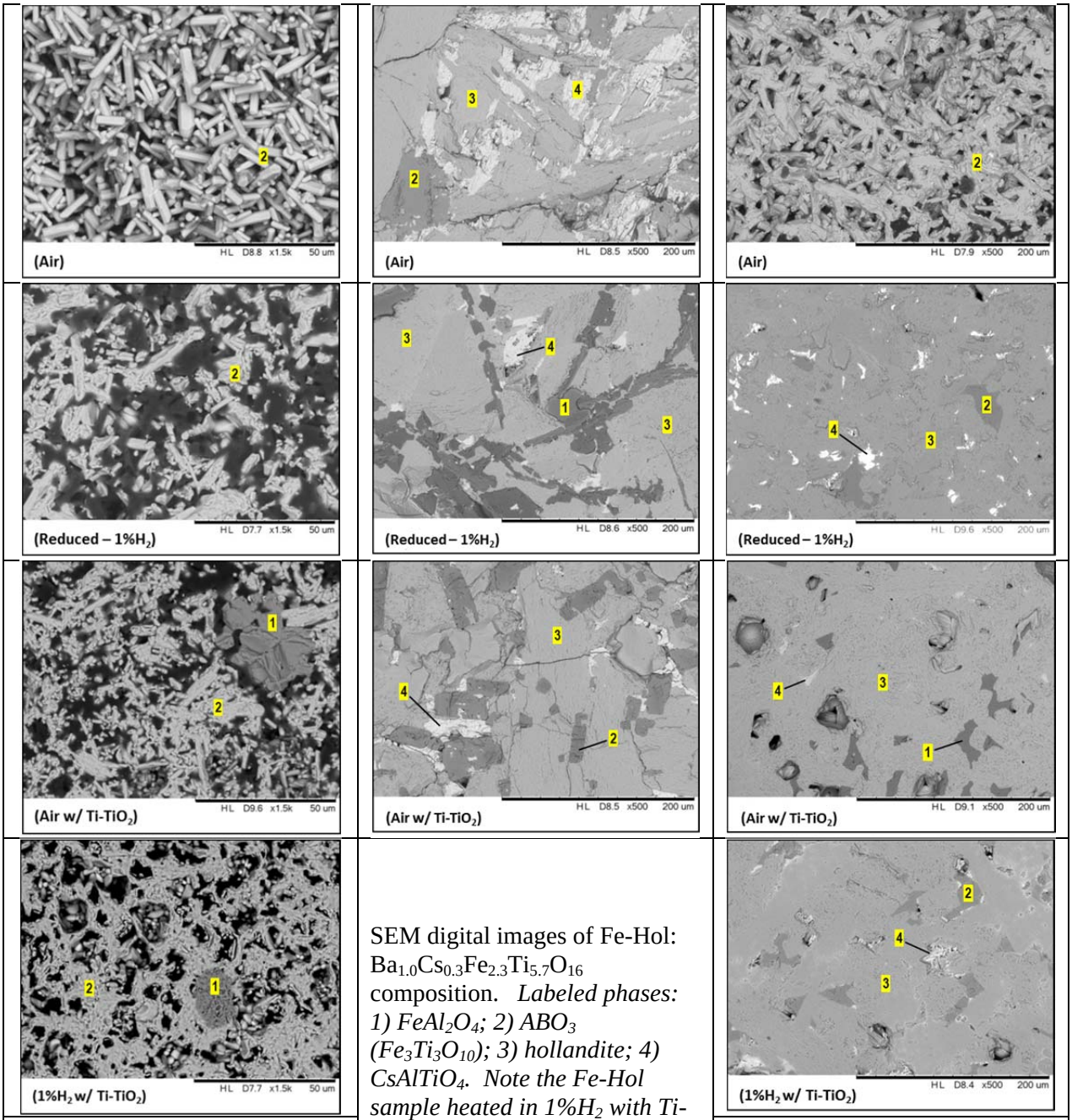

SEM digital images of Cr-Hol: $Ba_{1.0}Cs_{0.3}Cr_{2.3}Ti_{5.7}O_{16}$ composition. *Labeled phases: 1) rutile; 2) hollandite.*

SEM digital images of Fe-Hol: $Ba_{1.0}Cs_{0.3}Fe_{2.3}Ti_{5.7}O_{16}$ composition. *Labeled phases: 1) $FeAl_2O_4$; 2) ABO_3 ($Fe_3Ti_3O_{10}$); 3) hollandite; 4) $CsAlTiO_4$. Note the Fe-Hol sample heated in 1%H_2 with Ti-TiO_2 was unrecoverable from the furnace*

SEM digital images of CAF-Hol: $Ba_{1.0}Cs_{0.3}Cr_{1.0}Al_{0.3}Fe_{1.0}Ti_{5.7}O_{16}$ composition. *Labeled phases: 1) rutile; 2) Fe_2TiO_4; 3) hollandite; 4) $CsAlTiO_4$.*

Figure 4-1. SEM back scattered detector (BSD) digital images of single phase hollandite samples.

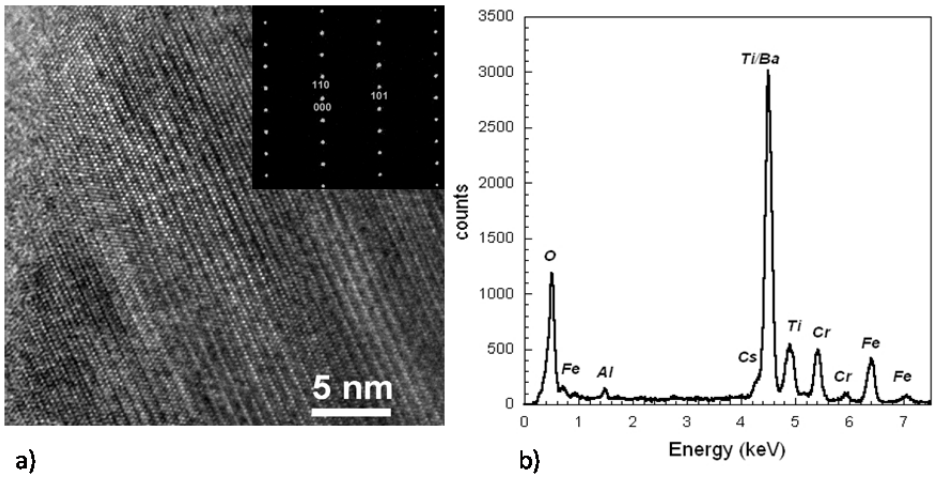

Figure 4-2. HRTEM image of CAF-SPH melted in Air without Ti/TiO_2 (inset SAD indexed to a tetragonal crystal structure) and b) chemical composition.

The SEM results further suggest that reducing agents and processing atmosphere affect hollandite formation and Cs incorporation. Under reducing conditions, melts batched with Fe_2O_3, would be rich in FeO and Al_2O_3 – either from the crucible or from the batch in the case of the CAF-Hol sample – and would precipitate the $FeAl_2O_4$ compound (observed in XRD) which is stable below 1820°C [12]. The resulting hollandite composition (relative to the starting hollandite) would be deficient in Fe and Al. Indeed, the reduced $FeAl_2O_4$ compound was observed in all Fe-containing samples heated in 1%H_2 whereas the Cr-Hol samples formed a single hollandite phase, under reducing or oxidizing atmospheres. Furthermore, as reduced $FeAl_2O_4$ compounds formed, the hollandite composition was driven off-stoichiometry, which in turn promoted several intermediate FeO-Fe_2O_3-TiO_2 compounds known to exist in equilibrium at or below the processing temperatures used in this research[13,14]. This effect was strongest in the Fe-Hol samples processed in reducing conditions without Ti/TiO_2 in which the high concentration of Fe combined with the low melting temperature increased the driving force for high-temperature secondary phase formation.

This research suggests that Cr preferentially enters the hollandite phase (even in the presence of competing phases). Due to its refractory nature, Cr does not form compounds readily with Cs and Cr^{3+} is not easily susceptible to reduction. Cr_2O_3 appears to stabilize the hollandite phase which in turn should promote Cs incorporation. This is visually observed in the SEM images by comparing the relative area of bright phase ($CsAlTiO_4$) across all samples and within each composition group.

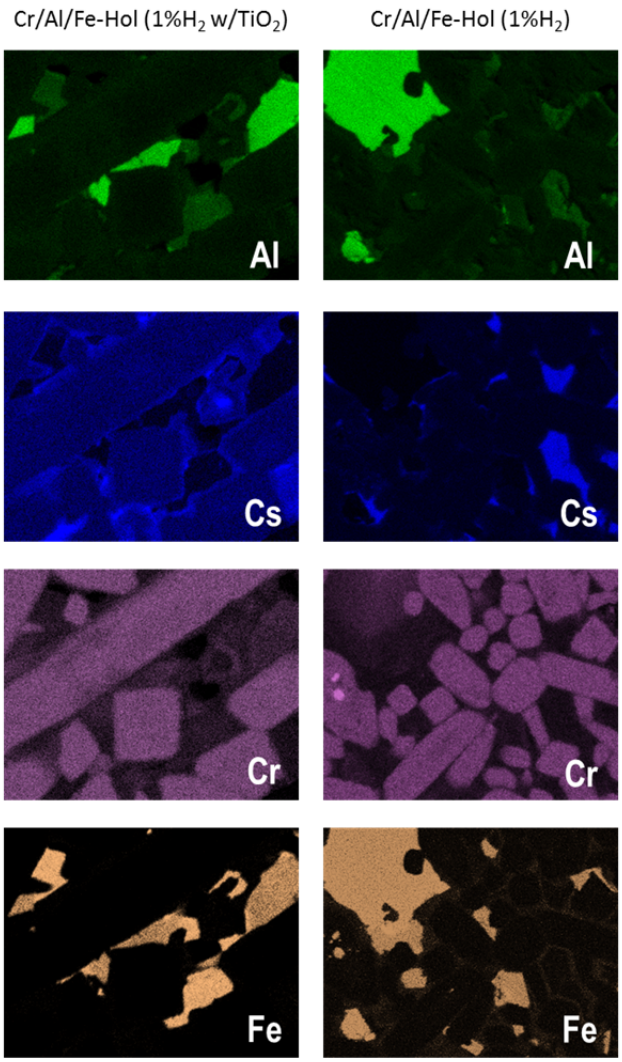

Figure 4-3. Select SEM-EDS elemental maps for CAF-Hol: $Ba_{1.0}Cs_{0.3}Cr_{1.0}Al_{0.3}Fe_{1.0}Ti_{5.7}O_{16}$ compositions heated under different reducing conditions.

4.4 X-ray absorption spectroscopy

X-ray absorption near edge spectroscopy (XANES) was used to confirm the average oxidation states of the Fe and the Cr in the CAF-Hol samples. Normalized XANES spectra are shown for Fe and Cr in Figure 4-4. XANES was used to identify changes in the average oxidation states of the Fe and the Cr resulting from the changes in composition and processing conditions. The Cr XANES and χ(R) EXAFS are identical within the experimental uncertainty, showing that Cr speciation is unaffected by the processing. The spectra are clearly those of Cr(III), not exhibiting the intense pre-edge peak characteristic of Cr(VI) that originates in the non-centrosymmetric environment of these species. Insofar as the original speciation is Cr(III) it is not surprising that processing under H_2 has no effect. The EXAFS display a high degree of order extending out through the fourth or fifth near neighbor shell. The Fe XANES clearly show a change in the

samples processed with H_2. The shift of the absorption edge to lower energy is consistent with the reduced species that would be expected to form under these conditions, with the extent of the shift within the range for the reduction of Fe(III) to (II). This change in speciation is also obvious in the EXAFS. The nearest neighbor peaks that represent the O shell are not only lower in amplitude but also shifted to higher R, with the second near neighbor peaks showing an even greater expansion in distance. The addition of the Ti appears to have minimal or negligible effects on the Fe speciation.

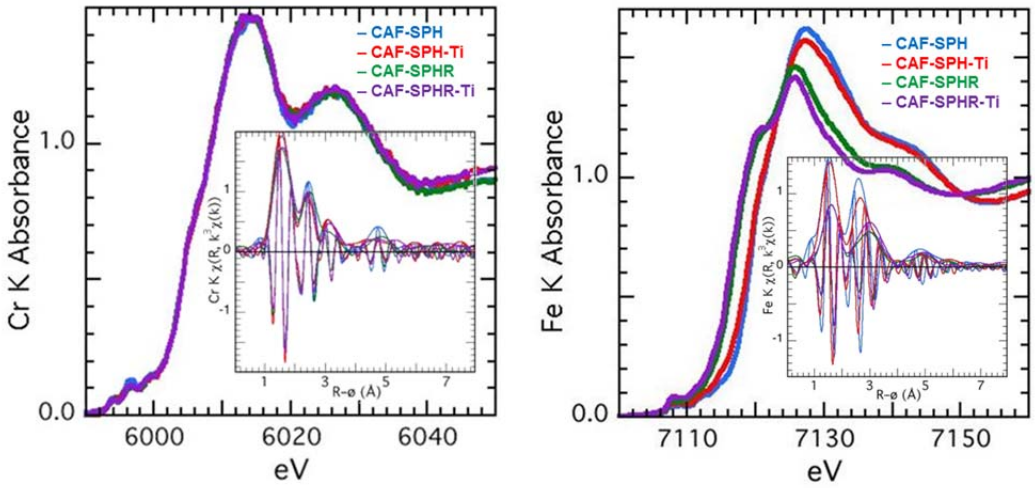

Figure 4-4. a) Cr and b) Fe XANES and EXAFS spectra of CAF-Hol: $Ba_{1.0}Cs_{0.3}Cr_{1.0}Al_{0.3}Fe_{1.0}Ti_{5.7}O_{16}$ processed in air (SPH); processed in air with Ti/TiO_2 (SPH-Ti); processed in 1%H_2 (SPHR); processed in 1%H_2 with Ti/TiO_2 (SPHR-Ti), according to the guide. The insets show the moduli and real components of the EXAFS in the χ(R) representation.

4.5 Durability Measurements

A standardized durability measurement has yet to be developed for multiphase ceramic waste forms. Leaching tests were performed to assess the comparative Cs retention between the three hollandite compositions synthesized under various processing conditions. The leaching test was intended to provide a qualitative measure of the Cs incorporation into the various hollandite compositions based on the assumption that parasitic Cs-rich phases control the initial Cs loss in leach tests. The measured Cs release was normalized to the measured surface area (0.1 – 0.4 m^2/g) for each sample. The Cs release across the samples for a given processing route was then normalized to one. The normalized Cs release summarized in Figure 4-5, indicated that the Fe-Hol sample exhibited the least Cs retention whereas the Cr-Hol sample exhibited the greatest Cs retention. The addition of Ti/TiO_2 appeared to increase the Cs retention in the Cr and CAF samples (to clarify, the increase was measured for the same processing atmosphere, not across air and 1%H_2). The Cs retention was greater in samples not heated under reducing conditions. This result can be understood considering the characterization results, which indicated reducing environments favor secondary phase formation that compete for Cs retention with the hollandite.

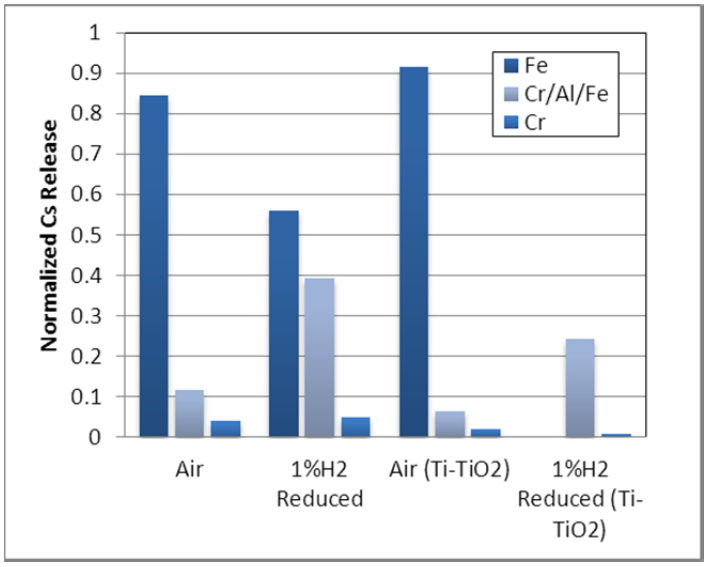

Figure 4-5. Normalized Cs release for Fe-Hol: $Ba_{1.0}Cs_{0.3}Fe_{2.3}Ti_{5.7}O_{16}$ (Fe), CAF-Hol: $Ba_{1.0}Cs_{0.3}Cr_{1.0}Al_{0.3}Fe_{1.0}Ti_{5.7}O_{16}$ (CAF), and, Cr-Hol: $Ba_{1.0}Cs_{0.3}Cr_{2.3}Ti_{5.7}O_{16}$ (Cr).

4.6 Summary

Processing in various redox conditions affected the phase purity of Fe-containing hollandites whereas had negligible effect on the resulting phase purity in the Cr-containing hollandites. X-ray absorption spectroscopy confirmed the relative stability of Cr^{+3} as compared to Fe^{+3} in various redox conditions. It is speculated that Cr helps to stabilize the hollandite phase during forming which in turn promotes Cs incorporation into the hollandite [7]. Durability studies indicated that Cr additions increased Cs retention and suppressed secondary phase formation compared to Fe-hollandite analogs. Hollandite compositions with Cr additions are considered a promising phase for Cs-immobilization and served as the basis for multi-phase ceramic waste form development and testing.

5.0 Multiphase Ceramic Crucible Studies

5.1 Calculation of Multi Phase Waste Form Compositions

Single phase hollandite compositions based on Cr and Cr/Al/Fe additions were incorporated into multiphase ceramics targeting hollandite, perovskite/pyrochlore and zirconolite phase assemblages. The phase assemblages were designed based on combinations of the waste and additives (the primary additive being TiO_2) to target the desired phases (i.e. hollandite, perovskite/pyrochlore and zirconolite) upon melting and subsequent cooling.

Table 5-1 summarizes two multiphase compositions (based on Cr and Cr/Al/Fe single phase hollandite studies) that were prepared, each with ~25 weight % waste loading and varying additive concentrations. Cr-MP denotes a multiphase assemblage targeting the Cr-hollandite analog and CAF-MP denotes a multiphase assemblage targeting the Cr/Al/Fe-hollandite analog. Multiphase samples were processed similarly to the single phase hollandite discussed in Section 4.1.

Table 5-1. Additive and waste concentrations (wt. %) of multiphase melt samples.

	Target wt. %		Target Phase
	CAF-MP	Cr-MP	
Waste	***24.66***	***24.58***	
BaO	2.20	2.20	**Cs-Hollandite** $(Ba_xCs_y)(Ti,Al)^{+3}_{2x+y}(Ti^{+4}_{8-2x-y})O_{16}$
CdO	0.11	0.11	-
Ce_2O_3	3.10	3.09	**(2+/3+) Titanate (i.e. Perovskite / Pyrochlore)** $(A^{2+})TiO_3$; $(A^{3+})_2Ti_2O_7$
Cs_2O	2.88	2.87	**(2+/3+) Titanate (i.e. Perovskite / Pyrochlore)** $(A^{2+})TiO_3$; $(A^{3+})_2Ti_2O_7$
Eu_2O_3	0.17	0.17	**(2+/3+) Titanate (i.e. Perovskite / Pyrochlore)** $(A^{2+})TiO_3$; $(A^{3+})_2Ti_2O_7$
Gd_2O_3	0.16	0.16	**(2+/3+) Titanate (i.e. Perovskite / Pyrochlore)** $(A^{2+})TiO_3$; $(A^{3+})_2Ti_2O_7$
La_2O_3	1.58	1.58	**(2+/3+) Titanate (i.e. Perovskite / Pyrochlore)** $(A^{2+})TiO_3$; $(A^{3+})_2Ti_2O_7$
MoO_3	0.85	0.84	-
Nd_2O_3	5.23	5.22	**(2+/3+) Titanate (i.e. Perovskite / Pyrochlore)** $(A^{2+})TiO_3$; $(A^{3+})_2Ti_2O_7$
Pr_2O_3	1.45	1.44	**(2+/3+) Titanate (i.e. Perovskite / Pyrochlore)** $(A^{2+})TiO_3$; $(A^{3+})_2Ti_2O_7$
Rb_2O	0.42	0.42	**Cs-Hollandite** $(Ba_xCs_y)(Ti,Al)^{+3}_{2x+y}(Ti^{+4}_{8-2x-y})O_{16}$
SeO_2	0.08	0.08	-
Sm_2O_3	1.08	1.07	**(2+/3+) Titanate (i.e. Perovskite / Pyrochlore)** $(A^{2+})TiO_3$; $(A^{3+})_2Ti_2O_7$
SnO_2	0.07	0.07	**(4+) Zirconolite** $CaZrTi_2O_7$
SrO	0.98	0.98	**(2+/3+) Titanate (i.e. Perovskite / Pyrochlore)** $(A^{2+})TiO_3$; $(A^{3+})_2Ti_2O_7$
TeO_2	0.66	0.65	-
Y_2O_3	0.63	0.63	**(2+/3+) Titanate (i.e. Perovskite / Pyrochlore)** $(A^{2+})TiO_3$; $(A^{3+})_2Ti_2O_7$
ZrO_2	2.99	2.98	**(4+) Zirconolite** $CaZrTi_2O_7$
Additive	***75.34***	***75.42***	
Al_2O_3	1.27	0.00	**Cs-Hollandite** $(Ba_xCs_y)(Ti,Al)^{+3}_{2x+y}(Ti^{+4}_{8-2x-y})O_{16}$
CaO	1.39	1.38	**(4+) Zirconolite** $CaZrTi_2O_7$
Cr_2O_3	6.33	14.50	**Cs-Hollandite** $(Ba_xCs_y)(Ti,Al)^{+3}_{2x+y}(Ti^{+4}_{8-2x-y})O_{16}$
BaO	10.56	10.52	**Cs-Hollandite** $(Ba_xCs_y)(Ti,Al)^{+3}_{2x+y}(Ti^{+4}_{8-2x-y})O_{16}$
Fe_2O_3	6.65	0.00	**Cs-Hollandite** $(Ba_xCs_y)(Ti,Al)^{+3}_{2x+y}(Ti^{+4}_{8-2x-y})O_{16}$
TiO_2	49.16	49.01	**Various**

5.2 Results

Multiphase research is ongoing but preliminary results indicate the feasibility of melt processing multiphase ceramics targeting an assemblage of titanate-based phases including hollandites of the form $Ba_{1.0}Cs_{0.3}A_{2.3}Ti_{5.7}O_{16}$; A = Cr, Fe, Al. XRD and SEM results indicated that the melt processing method produces similar phases obtained by alternative processing methods, namely zirconolite, perovskite, and pyrochlore structures. Figure 5-1 shows XRD patterns with phases identified for each sample. Processing in reducing atmosphere appeared to reduce un-desirable Cs-Mo containing phases, but at the same time promoted the formation of parasitic phases at the expense of the target hollandite, pyrochlore, and perovskite phases. Figure 5-2 is a SEM digital micrograph of a representative area of the CAF-MP sample. The results indicated highly substituted pyrochlore and perovskite phases that incorporated multiple lanthanides and transition metal species. The expected relative percentage of each phase was in agreement with bulk area analysis as shown in the table inset in Figure 5-2.

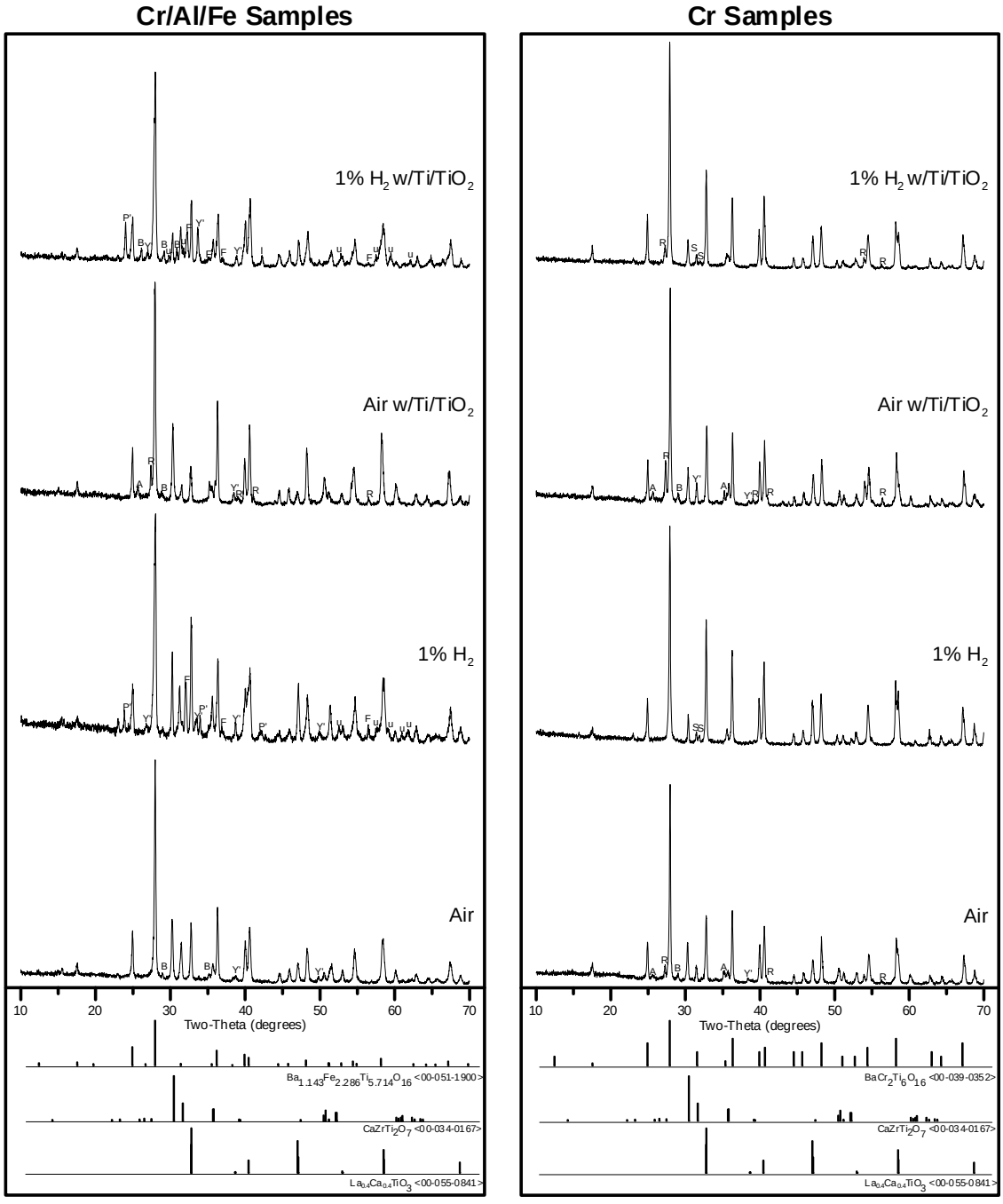

Figure 5-1. XRD patterns for multiphase ceramic compositions processed under varying conditions. The hollandite, perovskite, and pyrochlore phases were primarily identified via one of the three patterns shown. Additional phase were identified and are labeled in individual patterns. P') *perovskite-type*; Y') *pyrochlore-type*; R) TiO_2 – 00-021-1276; B) $Ba_7Al_2O_{10}$ – 00-041-0164; F)$BaFe_{12}O_{19}$ – 00-039-1433; I)FeO – 00-046-1312; A)Al_2O_3 – 00-046-1212; (S)$Sr_3Mo_2O_7$ – 00-052-1252. Unidentified peaks are labeled "u".

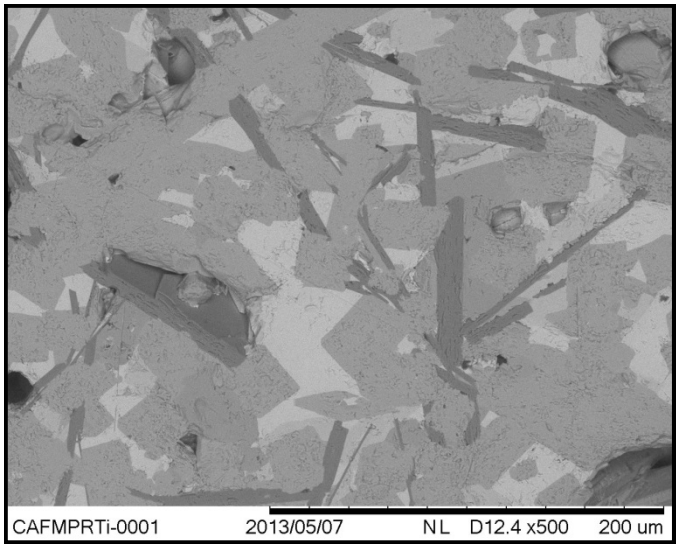

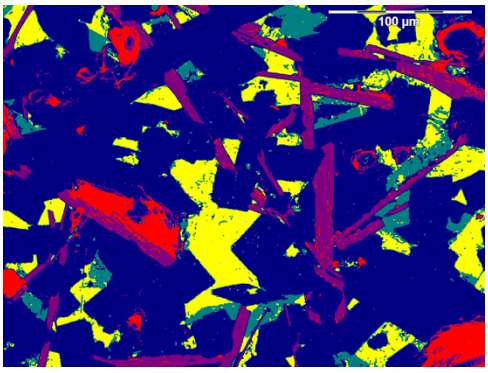

Region	Phase	Area %	Est. Vol. %
	Voids / porosity	4.6	4.6
	Hollandite	64.6	63.3
	RE-Pyrochlore	17.3	18.5
	Zirconolite	7.7	7.6
	Al-rich phase	5.9	-
	Perovskite/pyrochlore	-	6.0

Figure 5-2. SEM micrograph and corresponding area map of CAF-MP sample processed in 1%H_2 with added Ti/TiO_2 after cooling showing phase assemblage.

6.0 Path Forward or Future Work

6.1 Multiphase Composition and Property Development

Further research into the melting behavior, phase assemblage, and properties of multiphase ceramics is needed to establish the feasibility of these (or similar) ceramic compositions as hosts for nuclear waste from fuel reprocessing. The addition of Cr, although it appears to improve the property and performance of these ceramics, significantly increases the melting temperature and further composition development is needed to reduce the melting temperature. This work is currently being carried out with the goal of recommending a composition(s) for pilot-scale testing in a Cold Crucible Induction Melter (CCIM) to demonstrate melt processing. Subsequently, material produced in the CCIM will be characterized to make further improvement to the composition including processing parameters such as conductivity and cooling schedules.

6.2 CCIM Testing

Demonstration testing will be conducted on the Idaho National Laboratory (INL) CCIM test platform. The objective of the melter test campaign will be to demonstrate CCIM operations to process ceramics to include process initiation, initial pouring, and start/stop pouring. Melter parameters will be monitored over the duration of the testing to optimize the system. The crystallized ceramics will be characterized to determine bulk chemical composition, phase assemblage, and relative quality as measured by the PCT. Advanced characterization will also be performed to study cation partitioning (in each phase) and grain boundary features.

7.0 References

1. J. D. Vienna, "Nuclear Waste Vitrification in the United States: Recent Developments and Future Options," *International Journal of Applied Glass Science*, **1** [3] pp. 309-321, (2010).

2. A. E. Ringwood, S. E. Kesson, N. G. Ware, W. Hibberson and A. Major, "Immobilization of High-level Nuclear-Reactor Wastes in SYNROC," *Nature*, **278** [5701] pp. 219-223, (1979).

3. A. E. Ringwood, S. E. Kesson, N. G. Ware, W. O. Hibberson and A. Major, "SYNROC Process - Geochemical Approach to Nuclear Waste Immobilization," *Geochemical Journal*, **13** [4] pp. 141-165, (1979).

4. T. Advocat, G. Leturcq, J. Lacombe, G. Berger, R. A. Day, K. Hart, E. Vernaz and A. Bonnetier, "Alteration of Cold Crucible Melter Titanate-based Ceramics: Comparison with Hot-Pressed Titanate-based Ceramic," *Mater. Res. Soc. Symp. Proc*, **465** pp. 355-362, (1997).

5. I. A. Sobolev, S. V. Stefanovskii, B. I. Omelianenko, S. V. Ioudintsev, E. R. Vance and A. Jostons, "Comparative Study of Synroc-C Ceramics Produced by Hot-Pressing and Inductive Melting," *Mater. Res. Soc. Symp. Proc*, **465** pp. 371-378, (1997).

6. V. Aubin-Chevaldonnet, D. Caurant, A. Dannoux, D. Gourier, T. Charpentier, L. Mazerolles and T. Advocat, "Preparation and Characterization of $(Ba,Cs)(M,Ti)_8O_{16}$ ($M = Al^{3+}$, Fe^{3+}, Ga^{3+}, Cr^{3+}, Sc^{3+}, Mg^{2+}) Hollandite Ceramics Developed for Radioactive Cesium Immmobilization," *Journal of Nuclear Materials*, **366** [1-2] pp. 137-160, (2007).

7. J. W. Amoroso and J. C. Marra, "Ceramic Waste Form Data Package: Fuel Cycle Research and Development," *US Department of Energy Report Office of Nuclear Energy Separations and Waste Forms Campaign SRNL-STI-2014-00247 (FCRD-SWF-2014-000581),* Savannah River National Laboratory, Aiken SC (2014).

8. S. E. Kesson, "The Immobilization of Cesium in SYNROC Hollandite," *Radioactive Waste Management and Environmental Restoration*, **4** [1] pp. 53-72, (1983).

9. C. Biagioni, P. Orlandi and M. Pasero, "Ankangite from the Monte Arsiccio mine (Apuan Alps, Tuscany, Italy): occurrence, crystal structure, and classification problems in cryptomelane group minerals," *Periodico Di Mineralogia*, **78** [2] pp. 3-11, (2009).

10. R. W. Cheary and J. Kwiatkowska, "AN X-RAY STRUCTURAL-ANALYSIS OF CESIUM SUBSTITUTION IN THE BARIUM HOLLANDITE PHASE OF SYNROC," *Journal of Nuclear Materials*, **125** [2] pp. 236-243, (1984).

11. M. L. Carter, E. R. Vance, D. R. G. Mitchell, J. V. Hanna, Z. Zhang and E. Loi, "Fabrication, characterization, and leach testing of hollandite, (Ba,Cs)(Al,Ti)(2)Ti6O16," *Journal of Materials Research*, **17** [10] pp. 2578-2589, (2002).

12. K. Rosenbach, J. A. Schmitz and A. Eisenhuettenwes, *Eisenhuettenwes, 45 [12] pp. 843-47, (1974). Retrieved from ACerS-NIST Phase Equilibrium Diagrams, CD-ROM Database, Version 3.3.0, Figure 05152.*, pp.

13. J. B. MacChesney and A. Muan, *Am. Mineral., 44 [9-10] pp. 926-45 (1959). Retrieved from ACerS-NIST Phase Equilibrium Diagrams, CD-ROM Database, Version 3.3.0, Figure 00090.*, pp.

14. R. W. Taylor, *J. Am. Ceram. Soc., 46 [6] pp. 276-79 (1963). Retrieved from ACerS-NIST Phase Equilibrium Diagrams, CD-ROM Database, Version 3.3.0, Figure 02170.*, pp.